Video Article

Bioluminescence Imaging of NADPH Oxidase Activity in Different Animal Models

Wei Han[1], Hui Li[1], Brahm H. Segal[2,3], Timothy S. Blackwell[1]

[1]Department of Medicine, Vanderbilt University School of Medicine

[2]Departments of Medicine and Immunology, Roswell Park Cancer Institute

[3]Department of Medicine, University at Buffalo School of Medicine

Correspondence to: Wei Han at Wei.han@vanderbilt.edu

URL: http://www.jove.com/video/3925
DOI: doi:10.3791/3925

Keywords: Immunology, Issue 68, Molecular Biology, NADPH oxidase, reactive oxygen species, bioluminescence imaging

Date Published: 10/22/2012

Citation: Han, W., Li, H., Segal, B.H., Blackwell, T.S. Bioluminescence Imaging of NADPH Oxidase Activity in Different Animal Models. *J. Vis. Exp.* (68), e3925, doi:10.3791/3925 (2012).

Abstract

NADPH oxidase is a critical enzyme that mediates antibacterial and antifungal host defense. In addition to its role in antimicrobial host defense, NADPH oxidase has critical signaling functions that modulate the inflammatory response [1]. Thus, the development of a method to measure in "real-time" the kinetics of NADPH oxidase-derived ROS generation is expected to be a valuable research tool to understand mechanisms relevant to host defense, inflammation, and injury.

Chronic granulomatous disease (CGD) is an inherited disorder of the NADPH oxidase characterized by severe infections and excessive inflammation. Activation of the phagocyte NADPH oxidase requires translocation of its cytosolic subunits ($p47^{phox}$, $p67^{phox}$, and $p40^{phox}$) and Rac to a membrane-bound flavocytochrome (composed of a $gp91^{phox}$ and $p22^{phox}$ heterodimer). Loss of function mutations in any of these NADPH oxidase components result in CGD. Similar to patients with CGD, $gp91^{phox}$ -deficient mice and $p47^{phox}$-deficient mice have defective phagocyte NADPH oxidase activity and impaired host defense [2, 13]. In addition to phagocytes, which contain the NADPH oxidase components described above, a variety of other cell types express different isoforms of NADPH oxidase.

Here, we describe a method to quantify ROS production in living mice and to delineate the contribution of NADPH oxidase to ROS generation in models of inflammation and injury. This method is based on ROS reacting with L-012 (an analogue of luminol) to emit luminescence that is recorded by a charge-coupled device (CCD). In the original description of the L-012 probe, L-012-dependent chemiluminescence was completely abolished by superoxide dismutase, indicating that the main ROS detected in this reaction was superoxide anion [14]. Subsequent studies have shown that L-012 can detect other free radicals, including reactive nitrogen species [15, 16]. Kielland *et al.* [16] showed that topical application of **phorbol** myristate acetate, a potent activator of NADPH oxidase, led to NADPH oxidase-dependent ROS generation that could be detected in mice using the luminescent probe L-012. In this model, they showed that L-012-dependent luminescence was abolished in $p47^{phox}$-deficient mice.

We compared ROS generation in wildtype mice and NADPH oxidase-deficient $p47^{phox-/-}$ mice [2] in the following three models: 1) intratracheal administration of zymosan, a pro-inflammatory fungal cell wall-derived product that can activate NADPH oxidase; 2) cecal ligation and puncture (CLP), a model of intra-abdominal sepsis with secondary acute lung inflammation and injury; and 3) oral carbon tetrachloride (CCl_4), a model of ROS-dependent hepatic injury. These models were specifically selected to evaluate NADPH oxidase-dependent ROS generation in the context of non-infectious inflammation, polymicrobial sepsis, and toxin-induced organ injury, respectively. Comparing bioluminescence in wildtype mice to $p47^{phox-/-}$ mice enables us to delineate the specific contribution of ROS generated by $p47^{phox}$-containing NADPH oxidase to the bioluminescent signal in these models.

Bioluminescence imaging results that demonstrated increased ROS levels in wildtype mice compared to $p47^{phox-/-}$ mice indicated that NADPH oxidase is the major source of ROS generation in response to inflammatory stimuli. This method provides a minimally invasive approach for "real-time" monitoring of ROS generation during inflammation *in vivo*.

Video Link

The video component of this article can be found at http://www.jove.com/video/3925/

Protocol

1. Animal Models

1. Mice: Use p47$^{phox-/-}$ mice and age- and sex-matched C57BL6/DBA mice. Obtain approval for experiments from Institutional Animal Care and Use Committee.
2. Anesthesia: Use a continuous isoflurane administration system to induce anesthesia. The vaporizer system (VetEquip) is filled with isoflurane (2-3%). Confirm that mice are fully anesthetized by observing respiration, movement, and corneal reflex in response to external stimuli.
3. Surgical procedures: Scrub the surgical area (benchtop) with 70% ethanol. Wear sterile gloves and a clean surgical gown and mask. Prepare the mice by clipping the hair and applying betadine alternating with 70% ethanol to the area where the incision will be made. Perform surgery on a sterile surface and use sterile instruments. Monitor mice post-operatively until awake and moving freely.
4. Intratracheal zymosan administration
    1. Administer anesthesia as described in 1.2.
    2. Disinfect surgical area (neck) with betadine and 70% ethanol and expose the trachea by surgical dissection.
    3. Pierce trachea with a 27-gauge needle and inject zymosan (St. Louis, MO) at a dose of 1 µg/g using a 0.5 µg/µl solution (total volume 50 µl for a 25 g mouse) dissolved in sterile PBS.
    4. Close mice neck wound with 5-0 sterile silk sutures under aseptic conditions.
    5. Image after 4 hr and 24 hr.
5. Cecal ligation and puncture
    1. Administer anesthesia as described in 1.2.
    2. Clip hair in the surgical area (abdomen) and disinfect with betadine and 70% ethanol.
    3. Perform a midline laparotomy and identify the cecum.
    4. Ligate the distal 50% of exposed cecum with 4-0 silk suture and puncture cecum distal to the ligation with one pass of a 21-gauge needle.
    5. Close the incision with 4-0 sterile silk sutures.
    6. Image after 4 hr and 24 hr.
6. Oral carbon tetrachloride (CCl_4) administration
    1. Administer anesthesia as described in 1.2.
    2. Administer CCl_4 (2 µg/g, St. Louis, MO) dissolved in corn oil by oral gavage. The procedure of CCl4 administration should be performed in a designated area in accordance with IBC/EHS policies.
    3. Image after 4 hr and 24 hr.

2. Acquiring a Bioluminescent Image

1. Initialize the IVIS 200 (Xenogen Corporation, Alameda, CA) Imaging System, set to luminescence mode, and wait for the charge-coupled device (CCD) temperature to lock.
2. Select exposure time, binning (medium) and F/Stop (8) settings.
3. Place mice in supine position in the imaging chamber on a heated stage to maintain normal body temperature. Administer anesthesia as described in 1.2 via nose cone while mice are in the IVIS imaging chamber.
4. Administer L-012 (20 µg/g) dissolved in sterile PBS (10 µg/µl) intravenously via retro-orbital injection at each time point selected for imaging.
5. Capture images beginning at 2 min after L-012 injection. We typically use a 40 sec exposure.

3. Data Analysis using Region of Interest

1. Analyze data using Living Image software v.4.2 (Xenogen Corporation, Alameda, CA).
2. Open an image and select measurement of Region of Interest tools.
3. Select the Region of Interest shape and size over the chest or/and abdomen after overlaying a pseudo-colored digital image (representing photon detection) over a photographic image of the mouse.
4. Quantify signal intensity (photon flux) from the Region of Interest.

4. Statistics

1. Use statistical analysis software package to perform two-way ANOVA with Bonferroni post-testing at individual time points.

5. Representative Results

Zymosan is a pro-inflammatory yeast cell wall product and a potent activator of NADPH oxidase [3]. We previously showed that intratracheal zymosan induces a more robust neutrophilic lung inflammation and pro-inflammatory cytokine production in p47$^{phox-/-}$ compared to wildtype mice [1]. Here, our goal was to compare ROS generation in the lungs of wildtype and p47$^{phox-/-}$ mice following zymosan challenge. At 4 hr after intratracheal zymosan administration, we observed a significant increase in photon emission over the chest in wildtype mice compared to baseline as well as an increase in photon emission in wildtype compared to p47$^{phox-/-}$ mice at 4 h and 24 hr. In contrast, bioluminescence signals

in p47$^{phox-/-}$ mice remained at baseline levels at 4 hr after zymosan treatment (**Fig.1 A-B**). Thus, NADPH oxidase appears to be the major source of ROS generation in the lungs following zymosan administration.

Next, we assessed ROS production in the CLP-induced sepsis model. Sepsis is a life-threatening syndrome associated with end-organ injury, including acute lung injury (ALI) and acute respiratory distress syndrome (ARDS) [4, 5]. ROS-mediated injury has been considered to be an important factor driving sepsis-induced multi-organ dysfunction. We found that ROS were significantly increased over the chest (4 hr) and over the abdomen (24 hr) following CLP in wildtype mice compared to baseline. However, ROS levels in p47$^{phox-/-}$ mice were similar to baseline levels at both time points (**Fig.2 A-C**). These results show that ROS generation in the CLP-induced sepsis mouse model is NADPH oxidase-dependent.

Finally, we used bioluminescent imaging to detect ROS production in a CCl_4-induced liver injury model. CCl_4 causes hepatocellular necrosis, and has been used to model both acute liver injury and hepatic fibrosis [6]. In contrast to the previously described models of inflammation and injury, we found that ROS production in the abdomen was modestly (about 35%) increased over baseline in p47$^{phox-/-}$ mice at 4 h following CCl_4 administration. However, the magnitude of CCl_4-induced ROS generation was significantly greater in wildtype mice than in p47$^{phox-/-}$ mice (**Fig.3 A-B**). These data suggest that both p47^{phox} -containing NADPH oxidase-dependent and -independent ROS generation occur in acute CCl_4-induced liver injury.

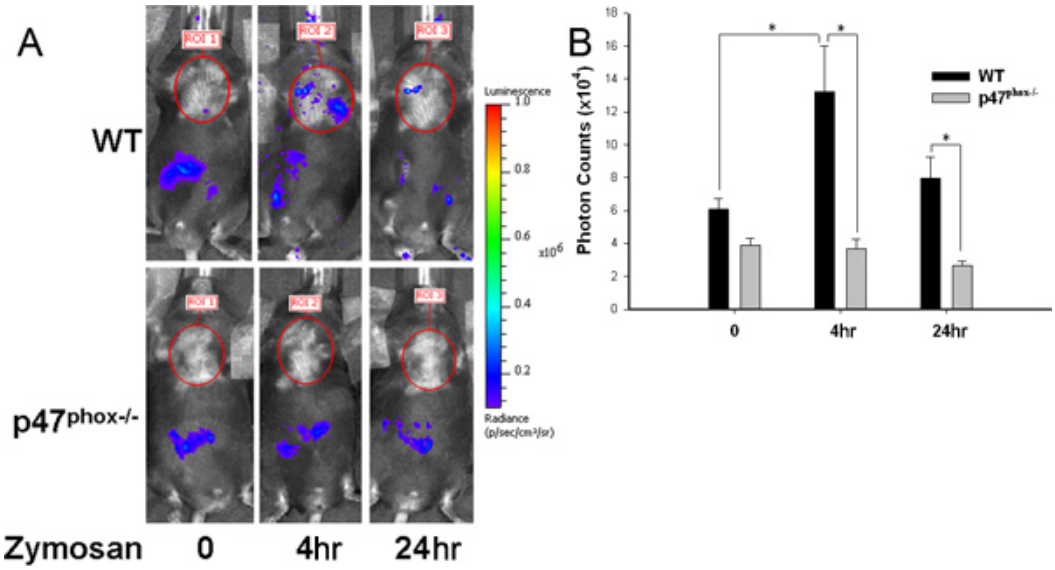

Figure 1. ROS production in lungs after zymosan treatment. A) Representative bioluminescence imaging of ROS production. Note that in addition to the chest, luminescence is detectable over the abdomen in both wildtype and p47$^{phox-/-}$ mice and abdominal luminescence is unchanged by zymosan treatment. B) photon counts from the chest of wildtype and p47$^{phox-/-}$ mice after a single intratracheal (IT) injection of zymosan. Bioluminescence imaging was performed at baseline, 4 hr, and 24 hr. Light emission from the region of interest over the chest was identified using the indicated pseudo-color scale. Results are presented as mean ± SE, n=6-9 per group, *=p<0.05. Click here for larger figure.

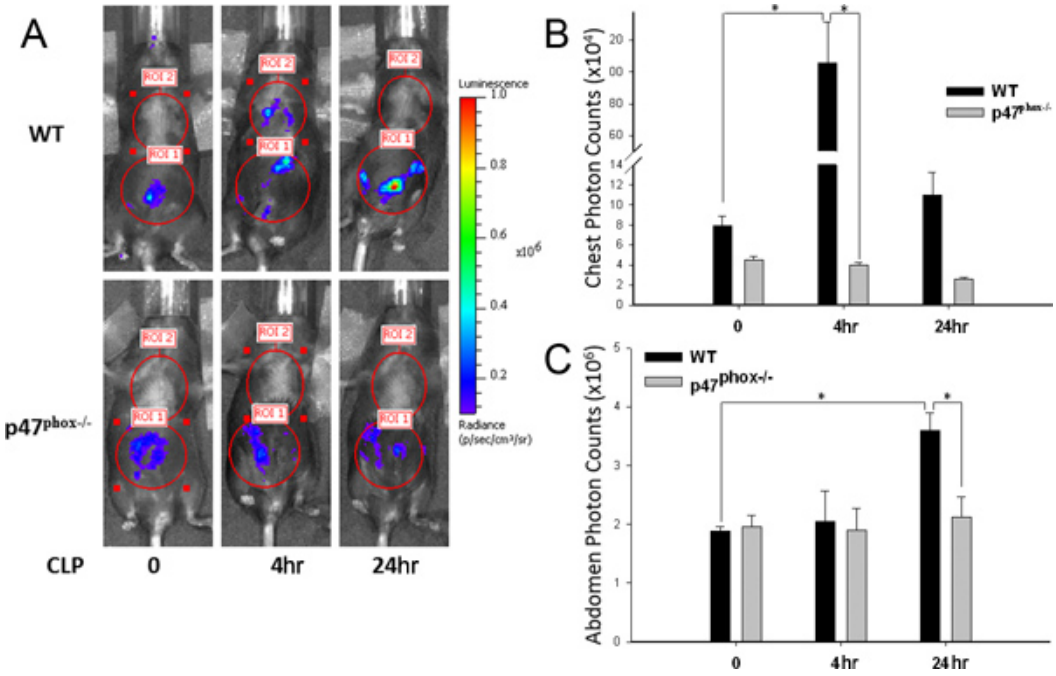

Figure 2. ROS detection following CLP. A) Representative bioluminescence imaging of ROS production, B) photon counts from the chest, and C) photon counts from the abdomen of wildtype and p47$^{phox-/-}$ mice at baseline, 4 hr, and 24 hr after CLP. Results are presented as mean ± SE; n=4-5 per group, *=p<0.05. Click here for larger figure.

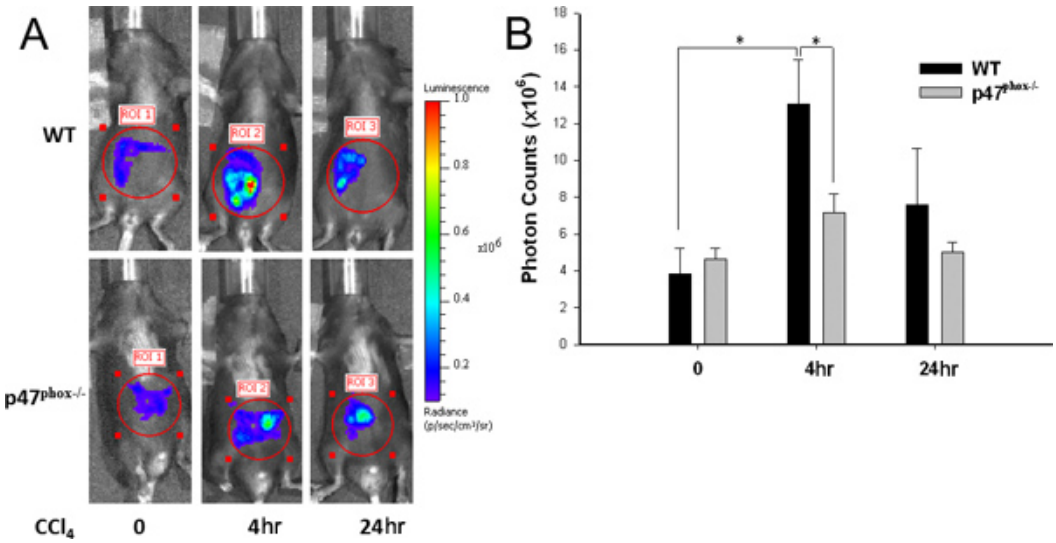

Figure 3. ROS production in abdomen after CCl_4-induced liver injury. A) Representative bioluminescence imaging of ROS production and B) photon counts from the abdomen of wildtype and p47$^{phox-/-}$ mice at baseline, 4 hr, and 24 hr after oral CCl_4 treatment. Results are presented as mean ± SE; n=4-5 per group, *=p<0.05. Click here for larger figure.

Discussion

"Real-time" measurement of reactive oxygen species (ROS) in living animals can be achieved by using fluorescent and chemiluminescent probes. While fluorescent probes suffer from having weak signal-to-noise ratios [12], the imaging technique described is more sensitive for detection of light emission following a chemical reaction of ROS with the luminol-based substrate L-012. Like all bioluminescent imaging techniques, this methodology is limited by wavelength-dependent light absorption and scatter by organs and tissues. These experiments were focused on establishing proper experimental conditions for the measurement of ROS in wildtype and p47$^{phox-/-}$ mice. The use of these genetically modified mice enables us to differentiate ROS generated by p47^{phox}-containing NADPH oxidase from ROS generated by other pathways.

Although functional NADPH oxidase containing $p47^{phox}$ is a major source of ROS, other NADPH oxidase isoforms exist, and additional ROS-generating systems, including xanthine oxidase and mitochondrial respiration, can produce ROS. NADPH oxidase and other ROS-generating pathways can have important and interactive effects on antimicrobial host defense and downstream signaling pathways that modulate inflammation and injury [7-10]. Using bioluminescence imaging, we were able to measure the kinetics of ROS production *in vivo* and to delineate the contribution of NADPH oxidase to ROS levels in different inflammatory models.

A limitation of this method relates to spatial resolution of bioluminescence. Although we can measure luminescence within specific anatomic compartments (*e.g.*, thorax, abdomen), it is difficult to localize the anatomic site of luminescence at the organ level. In each of our experimental models we chose 3 time points for bioluminescent measurements: baseline, 4 hr, and 24 hr. We do not know if bioluminescent imaging can identify small differences in ROS generation over shorter intervals of analysis or whether the relationship between *in vivo* ROS generation and bioluminescence is linear. These issues require further study. In the models used for these studies, we suspect that phagocytic cells, recruited neutrophils and macrophages, are primarily responsible for ROS production via the phagocyte NADPH oxidase system. Future studies in which specific cell types are depleted or bone chimeras are generated could provide additional knowledge about relative levels of ROS generation from different cell populations. Another potential limitation of studies using L-012 is that other radicals (besides ROS) may react with this luminescent probe, reducing specificity for ROS detection in some circumstances.

Following zymosan injection, the lack of ROS production in $p47^{phox-/-}$ mice indicates that NADPH oxidase is the major source of ROS in this model of lung inflammation. CLP is one of the most common animal models of sepsis [11] and bioluminescence imaging revealed increased ROS signals in both the lung and abdomen that were NADPH oxidase-dependent. In contrast to the zymosan and CLP models, ROS were increased in the abdomen of both of wildtype and $p47^{phox-/-}$ mice compared to baseline, but to a greater degree in wildtype mice, indicating that CCl_4 induces ROS production by $p47^{phox}$-containing NADPH oxidase and other mechanisms.

In summary, our data show that a luminol-based bioluminescence imaging method for the detection of ROS can be valuable tool for research on the regulation and consequences of ROS production *in vivo*.

Disclosures

No conflicts of interest declared.

Acknowledgements

This work was funded by NIH RO1 AI079253 and Department of Veterans Affairs.

References

1. Segal, B., Han, W. & Bushey, J. NADPH oxidase limits innate immune response in the lungs in mice. *PLoS ONE.* **5**, e9631 (2010).
2. Jackson, S., Gallin, J., & Holland, S.M. The p47phox mouse knock-out model of chronic granulomatous disease. *J. Exp. Med.* **182**, 751-758 (1995).
3. Gantner, B.N., Simmons, R.M., & Underhill, D.M. Collaborative induction of inflammatory responses by dectin-1 and Toll-like receptor 2. *J. Exp. Med.* **197**, 1107-1117 (2003).
4. Dejager, L., Pinheiro, I., & Libert, C. Cecal ligation and puncture: the gold standard model for polymicrobial sepsis. *Trends Microbiol.* **19**, 198-208 (2011).
5. Tsiotou, A.G., Sakorafas, G.H., & Bramis, J. Septic shock; current pathogenetic concepts from a clinical perspective. *Med. Sci. Monit.* **11**, RA76-85 (2005).
6. Fujii, T., Fuchs, B.C., & Tanabe, K.K. Mouse model of carbon tetrachloride induced liver fibrosis: Histopathological changes and expression of CD133 and epidermal growth factor. *BMC Gastroenterology.* **10**, 79-90 (2010).
7. Kubo, H., Morgensterm, D., & Doerschuk, C.M. Preservation of complement-induced lung injury in mice with deficiency of NADPH oxidase. *J. Clin. Invest.* **97**, 2680-2684 (1996).
8. Segal, B., Sakamoto, N., & Bulkley, G.B. Xanthine oxidase contributes to host defense against Burkholderia cepacia in the p47(phox-/-) mouse model of chronic granulomatous disease. *Infect Immun.* **68**, 2374-2378 (2000).
9. Droge, W. Free radicals in the physiological control of cell function. *Physiological reviews.* **82**, 47-95 (2002).
10. Jones, D. Radical-free biology of oxidative stress. American journal of physiology. *Cell physiology.* **295**, C849-868 (2008).
11. Hubbard, W.J., Choudhry, M., & Chaudry, I.H. Cecal ligation and puncture. *Shock.* **24**(s), 52-57(2005).
12. Wardman, P. Fluorescent and luminescent probes for measurement of oxidative and nitrosative species in cells and tissues: progress, pitfalls, and prospects. *Free Radic. Biol. Med.* **43**, 995-1022 (2007).
13. Pollock, J.D., Williams, D.A., & Gifford, M.A. Mouse model of X-linked chronic granulomatous disease, an inherited defect in phagocyte superoxide production. *Nat. Genet.* **9** (2), 202-209 (1995).
14. Nishinaka ,Y., Aramaki, Y., & Yoshida, H. A new sensitive chemiluminescence probe, L-012, for measuring the production of superoxide anion by cells. *Biochem. Biophys. Res. Commun.* **193**(2), 554-559 (1993).
15. Daiber, A., Oelze, M., & August, M. Detection of superoxide and peroxynitrite in model systems and mitochondria by the luminol analogue L-012. *Free Radic. Res.* **38**(3), 259-269 (2004).
16. Kielland, A., Blom, T., & Nandakumar, K.S. *In vivo* imaging of reactive oxygen and nitrogen species in inflammation using the luminescent probe L-012. *Free Radic. Biol. Med.* **47**(6), 760-766 (2009).

